Supplementary information for:
Synoptic- to meso-scale circulation connects fluvial and coastal gravel conveyors and directional deposition of coastal landforms in the Dead Sea basin

Haggai Eyal[1,2], Moshe Armon[1,3], Yehouda Enzel[1], Nadav G. Lensky[2,1]

[1]The Freddy & Nadin Herrmann Institute of Earth Sciences, The Hebrew University of Jerusalem, The Edmond J. Safra Campus, Givat Ram, Jerusalem 91904, Israel

[2]Geological Survey of Israel, 32 Yesha'yahu Leibowitz, Jerusalem 9371234, Israel

[3]Institute for Atmospheric and Climate Science, ETH Zurich, 8092 Zürich, Switzerland

Correspondence to: Haggai Eyal (haggai.eyal@mail.huji.ac.il) and Nadav G. Lensky (nadavl@gsi.gov.il)

S1 – Flash-floods

S1.1 Flash-floods dataset

The flash-floods dataset of Nahal Og for 2017-2022 is based on several sources summarized in Table S1. From this dataset we extracted:

(i) Flood occurrence according to the number of floods per hydrological year (a binary dataset).

(ii) Estimated flood magnitude according to pre-defined four classes: (a) low-flow floods, which due to transmission losses do not reach the lake, (b) weak floods, (c) moderate floods, and (d) large floods. Categorizing each flood to a specific class is by synthesizing direct field observations with (a) estimation of the highest stages from Time-Lapse Cameras (TLCs) and (b) reports from the Desert Floods Research Center (https://floods.org.il/english/ [in Hebrew]) as well as by social networks reports.

(iii) The timing of the first wave arrival to the lower reach of Nahal Og at the crossing of the Dead Sea highway (Road 90, location in Fig. 2b,c). This was determined for 8 floods (dark green in Table S1) by direct field observations or as recorded by TLCs (only for floods that occurred during the day). From these observations we calculated a typical lag of ~6 hours, on average, between the observed first wave of flood and the timing of the measured rain peak in Ma'ale Adumim (Location in Fig. 2b). We added this lag to the timing of rainstorms-producing floods peaks that their floods were not directly observed, to get the timing of their first waves. Typically for weak floods this lag time is longer, and for large floods it is shorter. Anyhow, these values were used only for plotting purposes as appear in Figs. 3 and 10.

Table S1: Nahal Og flash-floods for 2017-2022. TLC = time-lapse camera, SN= Facebook social network, SN-EG= Ein Gedi Field School reports, WHI= Israel Flash-flood Forecasting Center, Water Authority of Israel, DFRC= Desert Floods Research Center. Direct observation of the flood first wave by TLC during daylight are in dark green shade, estimated flood initiation during the night is by light green shade.

Flood No.	Floods per season	Rain peak(s)	First wave at Dead sea highway (Road 90)	Flood peak discharge category	Data sources and additional details
1	1	05/01/2018 15:00	05/01/2018 21:30	2	TLC (night), during-flood field visit, second wave at 12:00, end at evening
2	2	19/01/2018 1:00	19/01/2018 07:30	2	TLC (day), peak at 8:47, end at evening
3	3	26/01/2018 20:00	27/01/2018 01:00	1	TLC (night), end at 14:30
4	4	17/02/2018 23:00	18/02/2018 05:00	3	Post-flood field visit
5	5	26/04/2018 15:00	26/04/2018 21:00	3	Post-flood field visit
6	1	09/11/2018 11:00	09/11/2018 17:00	0	SN
7	2	22/11/2018 11:00	22/11/2018 17:00	1	During-flood field visit, end at night
8	3	06/12/2018 23:00	07/12/2018 05:00	1	SN
9	4	27/12/2018 9:00	27/12/2018 15:00	1	SN
10	5	16/01/2019 17:00	16/01/2019 23:00	2	SN, snow in JLM at 21:00
11	6	28/02/2019 9:00	28/02/2019 08:30	3	TLC (day), SN, peak at 9:30, second wave at 14:00, end at night
12	7	14/03/2019 9:00	14/03/2019 19:00	1	TLC (night), During-flood field visit, end at evening (17th)
13	1	09/12/2019 11:00	09/12/2019 19:00	1	TLC (night), DFRC
14	2	27/12/2019 4:00	27/12/2019 08:30	2	TLC (day), SN, second wave at 8:35
15	3	04/01/2020 22:00	05/01/2020 14:30	1	TLC (day), SN, end at evening
16	4	09/01/2020 3:00	09/01/2020 07:30	2	TLC (day), SN, second wave at 8:30
17	5	24/01/2020 1:00	24/01/2020 08:30	2	TLC (day), peak at 10:30, end at 18:00
18	6	08/02/2020 2:00	08/02/2020 18:00	1	DFRC
19	7	25/02/2020 11:00	25/02/2020 17:00	1	DFRC, SN (15:00 at Nebbi Musa)
20	8	06/03/2020 10:00	06/03/2020 17:00	2	DFRC, SN (14:00 at Nebbi Musa)
21	9	13/03/2020 13:00	14/03/2020 06:30	1	TLC (day), DFRC
22	1	05/12/2020 10:00	05/12/2020 19:00	1	DFRC, SN-EG (night)
23	2	16/12/2020 8:00	16/12/2020 14:00	1	DFRC, SN-EG
24	3	04/02/2021 15:00	04/02/2021 21:00	1	DFRC, SN, SN-EG
25	4	17/02/2021 20:00	18/02/2021 02:00	2	DFRC
26	1	20/11/2021 14:00	20/11/2021 20:00	0	DFRC, SN-EG
27	2	20/12/2021 15:00	20/12/2021 21:00	0	DFRC (22:30 at Nebbi Musa)
28	3	14/01/2022 13:00	14/01/2022 17:00	1	WHI (11:00 at Nebbi Musa,~15:00 at Almog)
29	4	16/01/2022 6:00	16/01/2022 10:00	2	WHI, SN-direct contact
30	5	27/01/2022 2:00	27/01/2022 06:00	3	TLC (night), end at evening
31	6	05/02/2022 0:00	05/02/2022 06:00	1	DFRC
32	7	19/02/2022 13:00	19/02/2022 19:00	0	DFRC

S1.2 Flash-flood hydrograph estimation

For the reconstruction of flood peak discharge, we collected field measurements of high-water marks (also observed in the TLC record), channel cross sections, estimation of the Manning's roughness value (0.35-0.04) and used the Manning formula with the approximation of a rectangular (or trapezoid for the narrower segment of the channel downstream of the knickpoint) channel cross section to estimate floods peak (Fig. S1, and Eyal et al., 2019). Then, we estimated the rest of the hydrograph using TLC snapshots from prior to and post the flood peak, marking of the change in water level and flow width and using the same procedure for discharge estimation by the Manning formula.

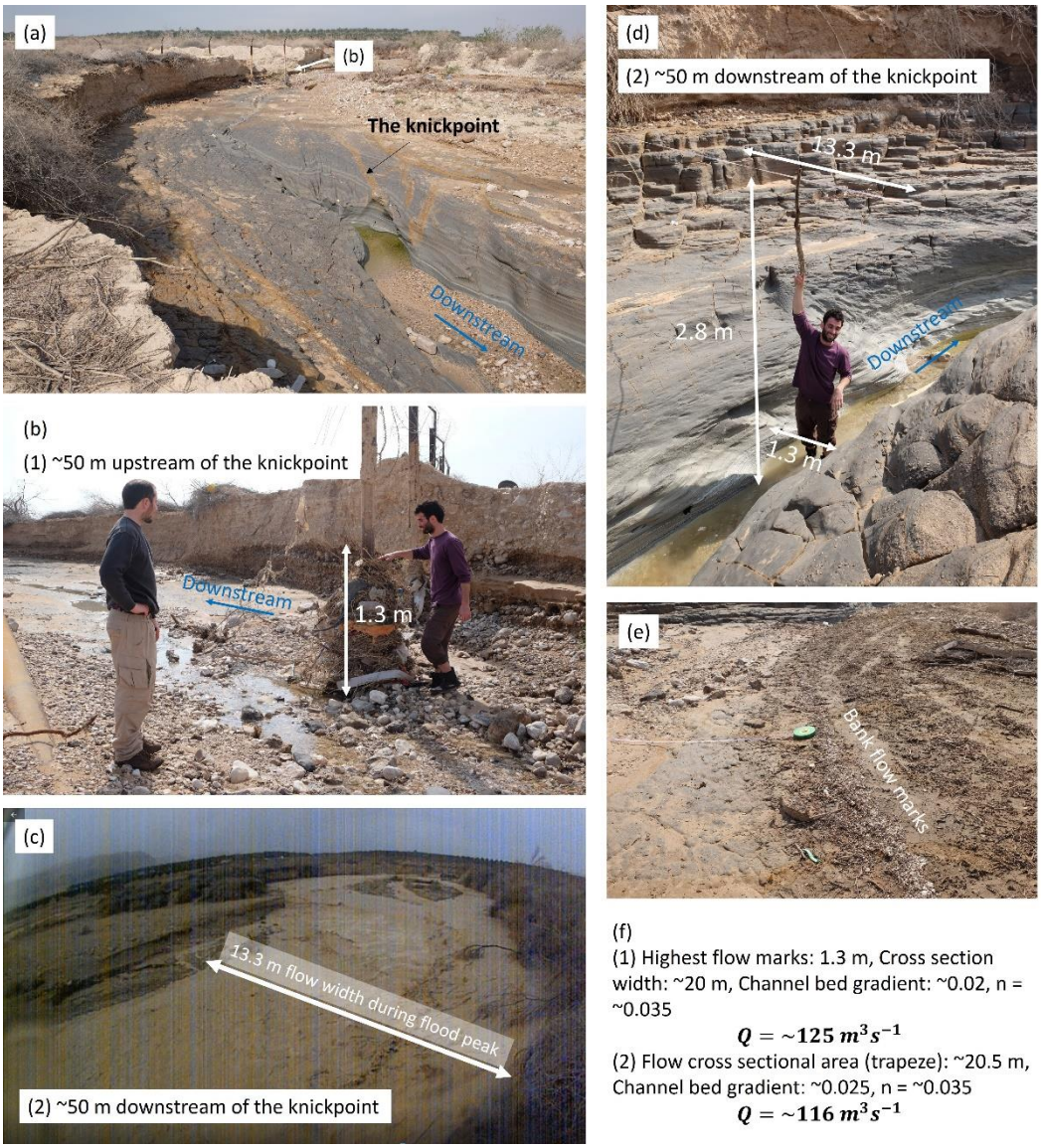

Figure S1: Reconstruction of the 27-Feb-2019 flood peak, the highest peak on our record (Fig. 8a). (a) The Nahal Og knickpoint (location is indicated in Fig. 2c) is incised into the lacustrine-laminated silt clay deposits of the shelf. (b) Measuring high watermarks on a metal pole located 50 m upstream the knikpoint. (c) TLC snapshot of the flood peak, looking upstream. The flow width during flood peak is indicated. (d) Estimation of the channel geometry using high flow marks that were left on the channel banks are shown in (e). (f) Calculation of the estimated peak discharge according to the parameters measured in the two locations.

S2 – Rainfall and wind climatic representation in the past three decades

A comparison of the rainfall and wind data with adjacent weather records of the past three decades, indicates that the five hydrological years explored in the manuscript well represent mean climatic conditions of the region.

According to the climatic atlas generated by IMS (https://ims.gov.il/he/ClimateAtlas [in Hebrew]), we compare the three decades (1991-2020) mean of rainfall for the three weather stations covering the Nahal Og watershed, with the annual rainfall of each hydrological year between 2017-2022 (Table S2). These years were either slightly wetter or slightly drier compared to the normal values, without a clear trend relative to the long term mean of annual rainfall.

Table S2: The multi-annual rainfall for the years 1991-2020 and the annual mean for hydrological years between 2017-2022 for Jerusalem center, Ma'ale Adumim and Kalia weather stations. Drier and wetter years/stations are marked by orange and green, respectively. Station locations are in Fig. 2b.

	Mean annual rainfall per hydrological year (mm) compared to the multi-annual mean (%)					
Name of rainfall gauging station	**1991-2020**	2017-2018	2018-2019	2019-2020	2020-2021	2021-2022
Jerusalem center	**522**	400 (77%)	644 (123%)	626 (120%)	421 (80%)	520 (99%)
Ma'ale Adumim	**276**	208 (75%)	331 (120%)	343 (124%)	263 (95%)	314 (114%)
Kalia (5 km south of Beit Ha'Arava	**94**	80 (85%)	92 (98%)	104 (111%)	69 (73%)	60 (64%)

A comparison of wind roses for Nahal Og (with almost five years of data, 2017-2022), with same time interval and a longer wind record (2008-2022) measured in Beit Ha'Arava nearby (Location in Fig. 2b), shows that the wind field of the two stations is rather consistent (Fig. S2).

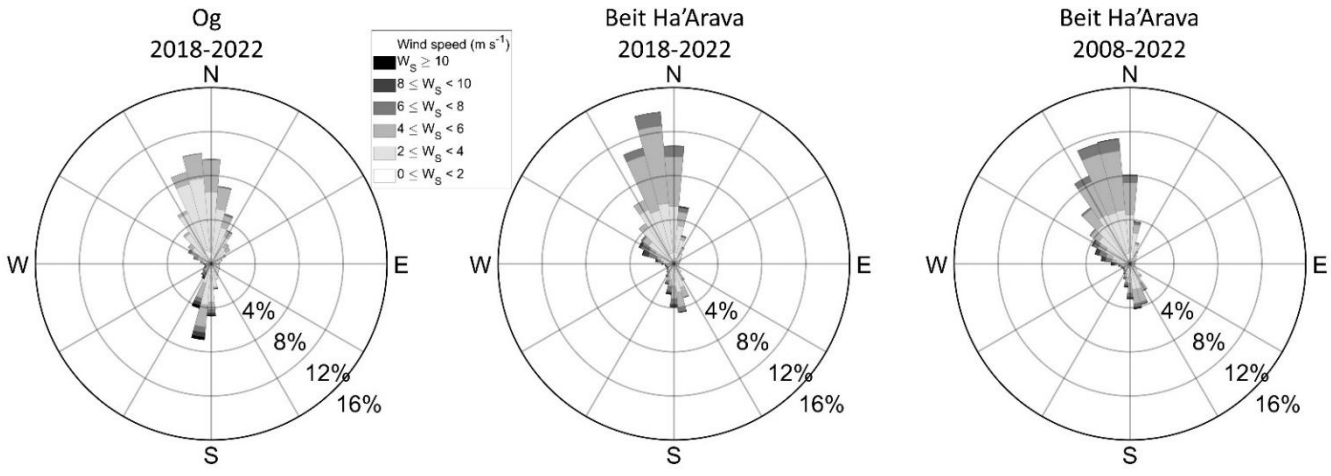

Figure S2: Wind roses for Nahal Og (left) for 2017-2022 and Beit Ha'Arava (middle) for the same time interval, and for a longer interval of Beit Ha'Arava of its full record since 2008 (right).

S3 – Significant wave height

We use continuous 4 Hz water pressure data to compute the significant wave height and period for specific storms using the OCEANLYZ toolbox (Karimpour and Chen, 2017). However, for the entire wave height record, which is sometimes incomplete, we use differences between maximum and minimum pressure at 10-min resolution as proxies for the significant wave height, which is normalized between 0 (no waves) to 1 (the highest wave). Figure S3 shows that this proxy can be taken as representative of the significant wave height by comparing it with the high-frequency analyzed data (by OCEANLYZ) and independent measurement of the significant wave height with an independent measurement using RBR-Solo-Wave pressure sensor.

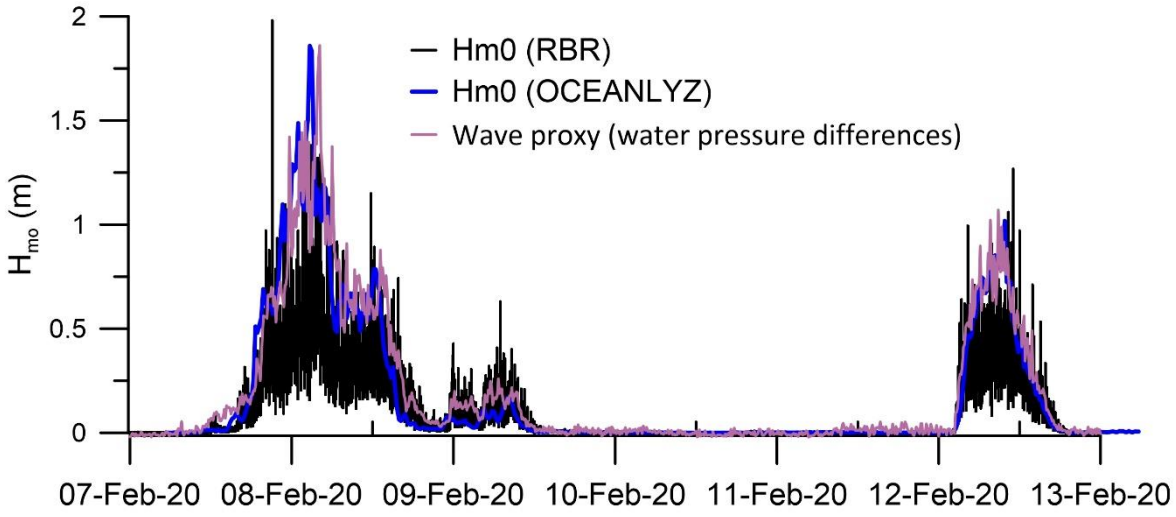

Figure S3: A comparison of the 'proxy significant wave height' with two independent datasets measured during the February 2020 'smart' boulders campaign of Eyal et al. (2021).

S4 – Synoptic maps and composites

The mean climatology of the four atmospheric circulation patterns (CPs) that prevail in the Dead Sea region and generated wind-wave storms is presented in Fig. S4. Mediterranean cyclones (MCs) are the dominant CP (~80% of the wind-wave storm population) generating the longest duration and highest intensity wind-wave storms. Red Sea Troughs (RSTs) constitute 15% of the population but generate mainly short duration and low intensity storms with synoptic-scale winds that approach the Dead Sea rift valley from the southeast (Fig. S4b) and then also funnelled inside the south-north elongated valley into southerlies. The remaining 5% of events are composed of Persian Troughs (PT) and Sharav Lows (SL). Details on the synoptic classification are in Sect. 3.2.

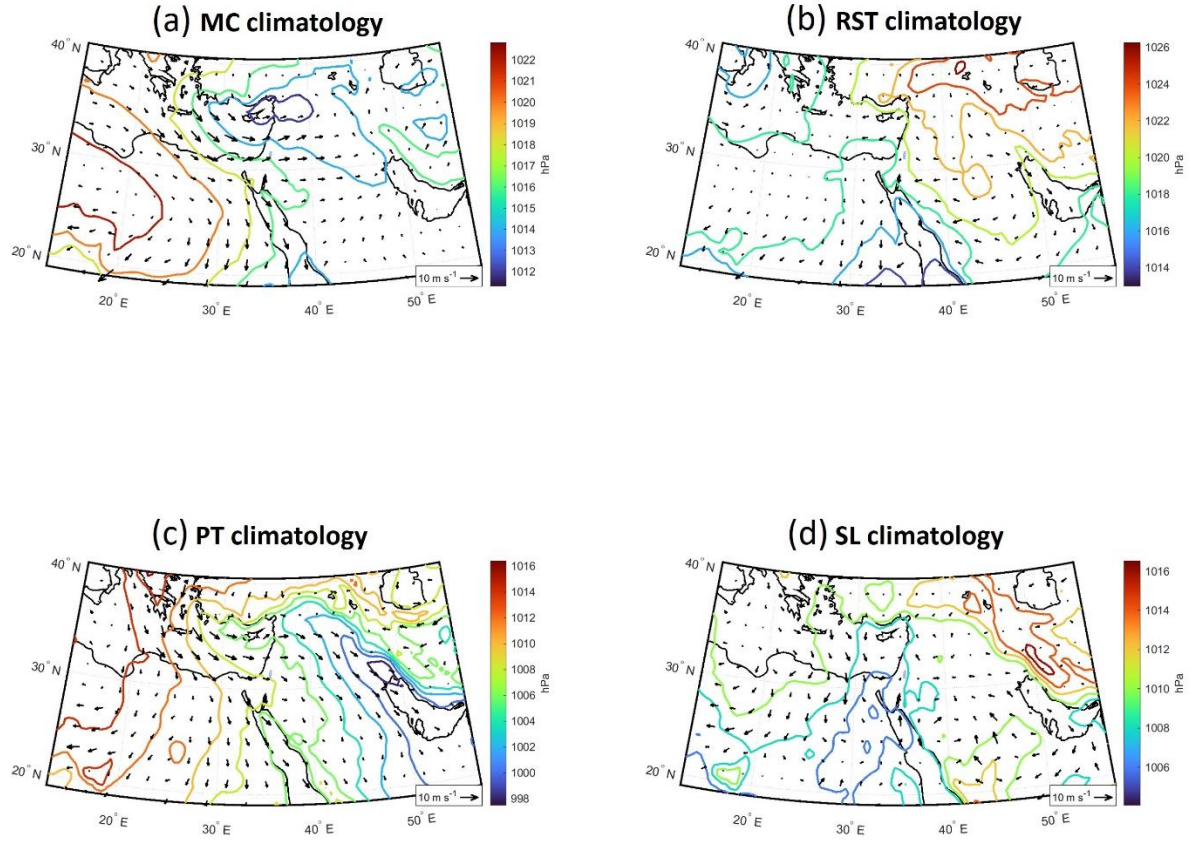

Figure S4: Mean climatology of the four CPs-producing wind-wave storms in the Dead Sea region. (a) MCs, (b) RSTs, (c) Persian troughs (PTs), and (d) Sharav Lows (SLs). Colored contours are mean sea level pressure, arrows are 10-m winds. Data is from ERA5 reanalysis (Hersbach et al., 2020).

The mean climatology of wind-wave producing storms according to the terciles of the storm wave energy shows how storms are of higher energy when MCs are deeper, centred over Cyprus or Syria and are accompanied by a high-pressure system from the south (Fig. S5).

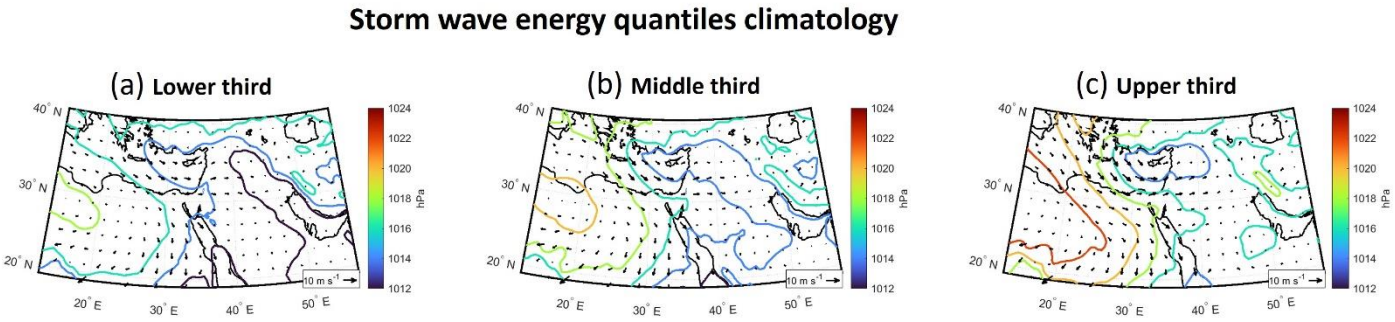

Figure S5: Same as Fig. S4, but for terciles of the storm wave energy. (a), (b), and (c) are the lower, middle, and upper thirds of the storm wave energy terciles.

S5 – Wind- driven waves

In the Deas Sea basin storm waves are wind driven; each one of the storm waves has a correlated/generating windstorm lasting similar duration (Fig. S6). Details on the classification into storms are in Sect. 3.2.

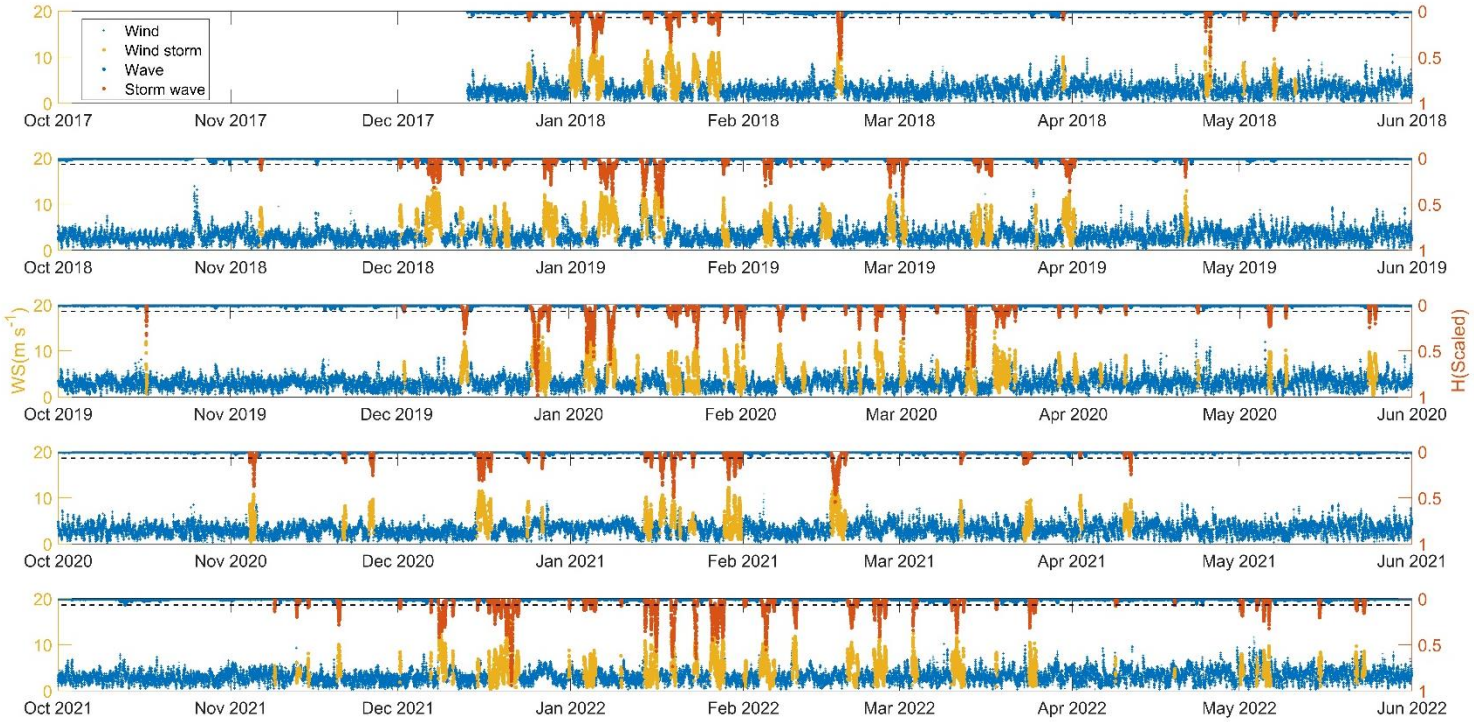

Figure S6: Wind driven wave storms during the five measured hydrological years 2017-2022 in Nahal Og meteorological station. 10-minutes raw data of wind and waves (blue crosses), windstorms (left axis; yellow), and storm waves (right reversed axis; orange).

S6 – Rainstorms-producing floods

Moderate or larger floods are generated by rainstorms with cumulative rainfall >10 mm storm^{-1} (Fig. S7).

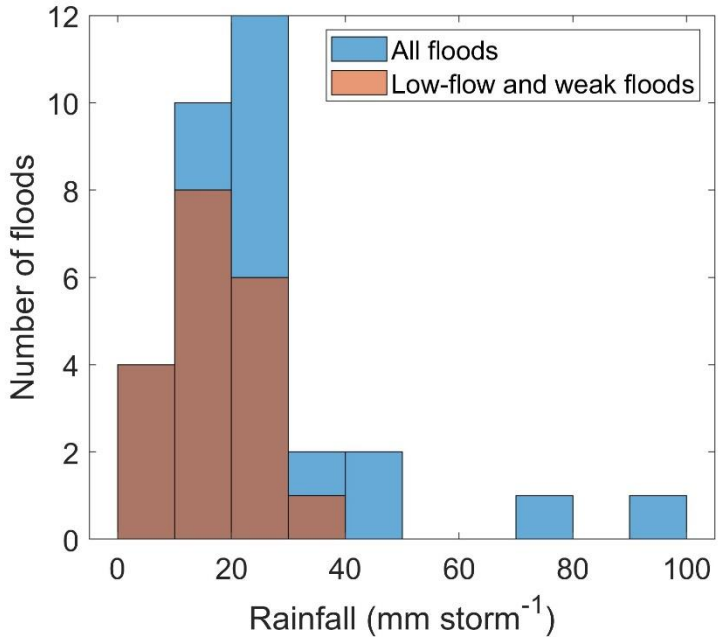

Figure S7: The distribution of flood-producing rainstorms. Note that moderate floods or larger are generated by >10 mm storm^{-1}, as measured in the center of the Nahal Og watershed in Ma'ale Adumim (location in Fig. 2b).

S7 – Asymmetry in deposition of fan-deltas

Here we provide additional examples for streams draining into the northwestern Dead Sea, preserving a pronounced northward deposition orientation of fan-deltas and paleoshorelines deposited under Late Pleistocene Lake Lisan highstand (Fig. S8).

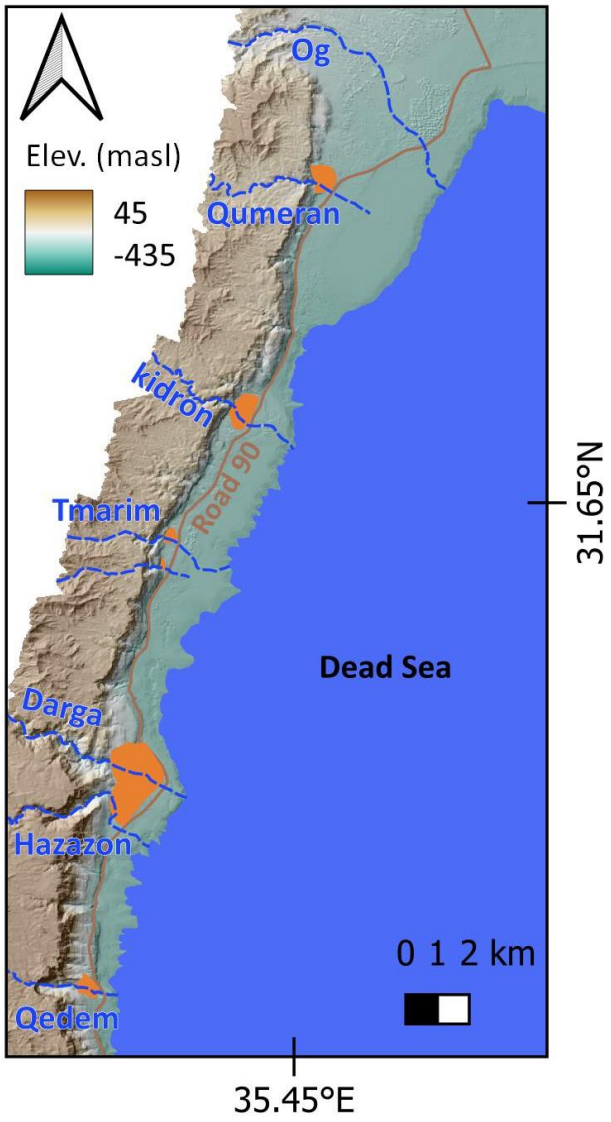

Figure S8: Map of the northwestern Dead Sea tributaries and their Late Pleistocene fan-deltas and paleo-shorelines deposited under Lake Lisan highstand (mapped in orange polygons). Note the deposition north to channel outlets from the Dead Sea western escarpment\cliff. The example of Nahal Tmarim is detailed in the main text (Sect. 5.3). The fan-deltas of Nahal Hazazon and Darga are mapped as one polygon due to their proximity, they coalesce; still, the main body of coarse sediment deposition for these two channels together is northern to their outlets from the cliff.

References

Eyal, H., Dente, E., Haviv, I., Enzel, Y., Dunne, T., and Lensky, N. G.: Fluvial incision and coarse gravel redistribution across the modern Dead Sea shelf as a result of base-level fall, Earth Surf. Process. Landforms, 44, 2170–2185, https://doi.org/10.1002/esp.4640, 2019.

Hersbach, H., Bell, B., Berrisford, P., Hirahara, S., Horányi, A., Muñoz-Sabater, J., Nicolas, J., Peubey, C., Radu, R., Schepers, D., Simmons, A., Soci, C., Abdalla, S., Abellan, X., Balsamo, G., Bechtold, P., Biavati, G., Bidlot, J., Bonavita, M., Chiara, G., Dahlgren, P., Dee, D., Diamantakis, M., Dragani, R., Flemming, J., Forbes, R., Fuentes, M., Geer, A., Haimberger, L., Healy, S., Hogan, R. J., Hólm, E., Janisková, M., Keeley, S., Laloyaux, P., Lopez, P., Lupu, C., Radnoti, G., Rosnay, P., Rozum, I., Vamborg, F., Villaume, S., and Thépaut, J.: The ERA5 global reanalysis, Q. J. R. Meteorol. Soc., 146, 1999–2049, https://doi.org/10.1002/qj.3803, 2020.

Karimpour, A. and Chen, Q.: Wind wave analysis in depth limited water using OCEANLYZ, A MATLAB toolbox, Comput. Geosci., 106, 181–189, https://doi.org/10.1016/j.cageo.2017.06.010, 2017.